ABAQUS-Based Uniaxial Compression Performance Study of CFRP-SC Columns

Qingxin Li, Han Xiao *

Civil Engineering, Dalian Maritime University, Dalian, China, 116026

* Corresponding Author Email: hzzldbbt@163.com

Abstract. With the increasing shortage of sand resources for construction, sea sand has become its emerging alternative. However, since sea sand can lead to the deterioration of concrete structures, it is particularly important to design a corrosion-resistant, efficient, green, convenient, and low-cost reinforcement method. Carbon fiber reinforced composites (CFRP) with corrosion resistance and high strength can enhance the mechanical properties and durability of sea sand concrete structures (SC). In this paper, ABAQUS subroutine VUSDFLD is used for secondary development, combined with unit deletion algorithm and maximum tensile stress criterion to establish a uniaxial compression damage model, to analyze the damage effect of uniaxial compression state of CFRP-Sea Sand Concrete Column (CFRP-SC). The results show that: (1) CFRP fibers can effectively improve the compressive and load-bearing capacity of SC, thus reducing the stress concentration phenomenon when the column is under compression. (2) The damage evolution of CFRP-reinforced SC under uniaxial pressure is slower, and the high strength of CFRP fibers can effectively resist crack expansion and slow down the damage process of the column.

Keywords: CFRP fiber reinforcement, SC, Single-axis press performance, ABAQUS, Secondary development.

1. Introduction

At present, with the continuous expansion of China's construction scale, the demand for sand is rising year by year, the uncontrolled exploitation and waste of river sand resources caused by river diversion, serious water infiltration and other problems, has seriously affected the people's practical life and health and safety. And the consumption of freshwater resources is large, so the use of sea sand to prepare new SC has become a hot research topic for many scholars. The concrete prepared by using sea sand as raw material has already achieved some practical applications in engineering. For example, Hong Kong's airport and Shanghai Baosteel Group's Maanshan Port are successful cases of utilizing sea sand as raw material. However, the salt content of sea sand is higher than that of freshwater sand, which leads to problems such as hydration reaction and corrosion of reinforcement in SC [1].

Fiber-reinforced composites (FRP) have been widely used in the field of civil engineering structural reinforcement due to their advantages of light weight, high strength, corrosion resistance, good fatigue resistance and convenient construction [2]. It is found that FRP pasted on the surface of concrete beams can not only improve its ultimate load carrying capacity, but also improve its stiffness, which has a good effect of reinforcement and repair [3].The use of FRP as a reinforcing material for seawater SC structures has attracted extensive attention at home and abroad, and has become an important direction of expansion in the field of civil engineering and a hotspot of research in the academic community at home and abroad. So far, many scholars have used FRP fibers to reinforce SC structures and have achieved many results [4-7].

Chen study investigated the effect of CFRP on the load carrying capacity, deformation capacity and durability of concrete filled FRP pipe columns using axial compression tests and numerical simulation. The results of the study showed that CFRP reinforcement can significantly improve the load carrying capacity and durability of concrete filled FRP pipe columns and can enhance the deformation capacity and stability of the columns [8]. Wu study experimentally investigated the axial compression behavior of glass fiber reinforced polymer tubes with CFRP restraints. The results show

that CFRP restraint can significantly improve the load carrying capacity and ductility of glass fiber reinforced polymer pipe columns and can effectively control the crack extension of the columns. In addition, CFRP reinforcement can also improve the shear strength and toughness of the column [9]. Shi study conducted behavioral experimental studies on CFRP-restrained square steel-tube concrete infill columns. The results of the study showed that CFRP confinement was able to significantly improve the load carrying capacity and ductility of square steel tubular concrete infill columns. At the same time, CFRP reinforcement can also effectively prevent the column from shear damage when subjected to lateral loads [10].

For FRP materials, there are four main types of FRP commercial materials, namely glass fiber reinforced composites (GFRP), carbon fiber reinforced composites (CFRP), aramid fiber reinforced composites (AFRP), and basalt fiber reinforced composites (BFRP), which can be readily applied in concrete [11]. However, aramid FRP fibers are expensive and have a high relaxation rate, glass FRP fibers have low tensile strength [12], and the modulus of elasticity of glass fiber-reinforced composite (GFRP) tendons and basalt fiber-reinforced composite (BFRP) tendons is low, about a quarter of that of steel [13].

Therefore, the carbon fiber composite (CFRP reinforcement), which has the most superior comprehensive performance, is selected as the external reinforcement of SC (SC) in this project. In this study, the secondary development of ABAQUS with Fortran compiler was utilized to investigate the damage evolution law of CFRP-SC subjected to external loading, which provides useful guidance for the improvement of SC structural reinforcement technology.

2. Model building

2.1. SC modeling

A finite element model of SC with dimensions of 150 mm × 150 mm × 300 mm was established using ABAQUS software (Fig. 1). The density of the material was 2195 kg/m3, the modulus of elasticity E=34.5 GPa, and Poisson's ratio μ=0.20 (Table 1). The model was analyzed by display dynamic analysis method, and a total of 54000 meshes were divided, and the mesh type was C3D8R. The model was fixedly constrained at the bottom, and the top surface was loaded by displacement, with the maximum displacement of 45 mm, and the loading rate was 0.1 mm/s (Fig. 2). In the model, the Y-axis direction is vertical, and the X and Z axes are horizontal. In the calculation range, the model is each homogeneous.

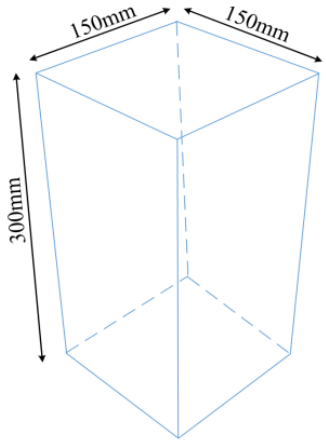

Figure 1. Calculation model

Figure 2. Mesh model

Table 1. SC mechanical properties

	ρ(kg/m^3)	E(GPa)	μ
SC	2195	34.5	0.20

2.2. CFRP-SC modeling

The size of the CFRP-SC model is 150 mm × 150 mm × 300 mm (Fig. 3). The density of the CFRP material is 7076 kg/m3, the modulus of elasticity E=230 GPa, and Poisson's ratio μ=0.20 (Table 2). The thickness of the CFRP fibers is 0.5 mm, the length is 150 mm, and the width is 15 mm. The type of the model mesh is C3D8R, and the model is divided into a total of 14782 cells. In the uniaxial compression simulation, vertical constraints were applied to the bottom of the model and displacement-controlled compression was applied to the top surface. The maximum displacement of loading was 45mm, and the loading rate was controlled at 0.1mm/s (Fig. 4).

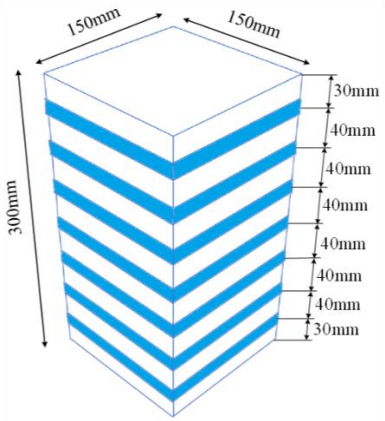

Figure 3. Calculation model

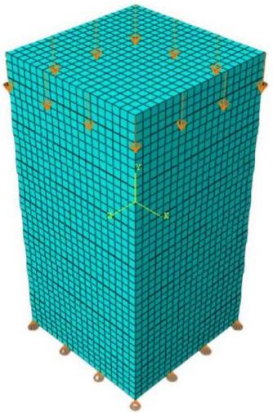

Figure 4. Mesh model

Table 2. CFRP mechanical properties

	ρ(kg/m^3)	E(GPa)	f_t(MPa)	μ
CFRP	7076	230	400	0.20

2.3. Element deletion algorithm

The element deletion function itself is a method to overcome the shortcomings of the finite element itself. Since the finite element itself is based on continuum mechanics, and in continuum mechanics the object under study needs to be continuous, i.e. the material domain is continuous in space. In the framework of such theoretical assumptions, the unit itself does not disappear, and the deletion of the unit is associated with damage, and the mechanism of damage can generally be summarized in two cases, i.e., tensile damage and shear damage. However, in the actual situation, due to the existence of damage fracture, will inevitably make some units disappear or completely failed, so to be able to simulate this situation, ABAQUS software platform provides unit deletion function for use.

Consider the rod shown in Fig. 5(a), which is stretched from its original position AB and rotated to the new position A'B'. This deformation can be realized in two stages: first the rod is stretched, as shown in Fig. 5(b). Then it is rotated by applying a rigid body rotation to it, as shown in Fig. 5(c). The stress in the rod after stretching is, which is constant during the rigid body rotation. The coordinate system rotated due to the rigid body rotation is a co-rotating coordinate system. Therefore, the stress tensor and state variables are calculated directly [14].

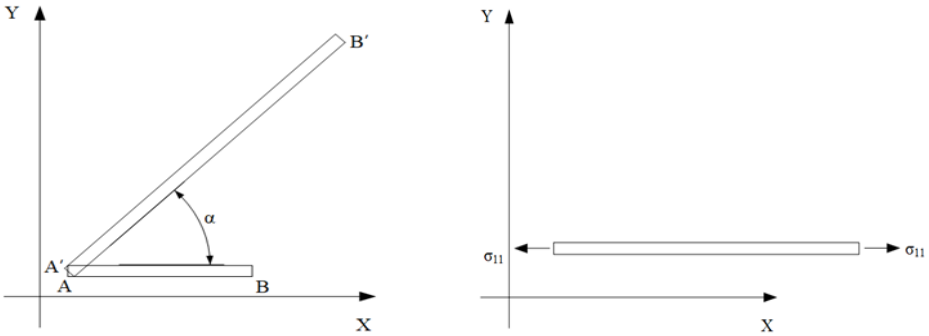

(a) Rod position transformation diagram (b) Rod tensile diagram

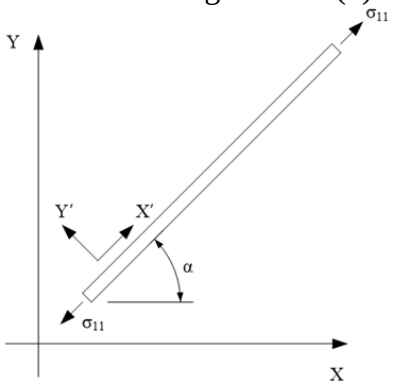

(c) Rod rotation diagram

Figure 5. Schematic diagram of unit deletion method

2.4. Maximum tensile stress damage criterion

The maximum tensile stress criterion, also known as the maximum yield stress criterion, is a typical damage criterion used to evaluate composite materials. It is a damage criterion that takes the maximum stress (or yield stress) as a criterion and considers the overall condition of the structure to determine the safety of the structure. When the actual stress reaches a certain value, the material can be damaged. The maximum tensile stress criterion is a damage criterion based on physical principles, and it is a criterion for evaluating the safety of a member based on its deformation under stress. The

basic principle of the maximum tensile stress criterion is that when the stress exceeds a certain value, the material can be damaged. Therefore, in practice, it is only necessary to ensure that the stress does not exceed a certain value to ensure the safety of the structure.

Guidelines for maximum tensile stress in a unit:

$$f = |\sigma_1| - \sigma_t \tag{1}$$

2.5. Concrete damage destruction model (CDP model)

In the CDP model, the uniaxial tensile and compressive responses of concrete are characterized by damage plasticity, and the relevant parameters of the CDP model are calculated using the Code for Structural Design of Concrete (GB50010-2010) [15] (Table 3).

Table 3. CDP model parameters

Compressive strength (MPa)	Inelastic strain ($\times 10^{-3}$)	Factor of damage d_c	Tensile strength (MPa)	Strain of cracking ($\times 10^{-3}$)	Tensile damage factor d_t
21.06015	0	0	2.11284	0	0
22.68367	1.862E-05	0.0026755	2.64	1.965E-05	0.0611993
24.31216	4.307E-05	0.01009253	2.50677	4.634E-05	0.14635663
25.93727	7.508E-05	0.02192468	2.37329	6.202E-05	0.1958968
27.55771	0.00011767	0.03840388	2.23975	7.65E-05	0.24108453
29.19453	0.00017771	0.06104518	2.10591	9.081E-05	0.28478415
30.82572	0.00027074	0.09364065	1.97307	0.00010528	0.32767213
32.4	0.00055351	0.17846276	1.83938	0.00012046	0.37092191
30.76493	0.00090922	0.2616336	1.70595	0.00013654	0.4145507
29.12673	0.00111615	0.30483303	1.57339	0.00015379	0.45860408
27.48783	0.00130692	0.3431696	1.44038	0.00017283	0.5037065

The CDP model is combined with the cell deletion algorithm to delete cells without carrying capacity. When utilizing the cell deletion algorithm, the state variable should be set to a value of 1 or 0. A value of 1 indicates that the cell is active, while a value of 0 indicates that the cell is disabled and deleted (Fig. 6 and Fig. 7).

Sabotage criterion:

$$\bar{\varepsilon}_c^{pl} \geq 0.05 \tag{2}$$

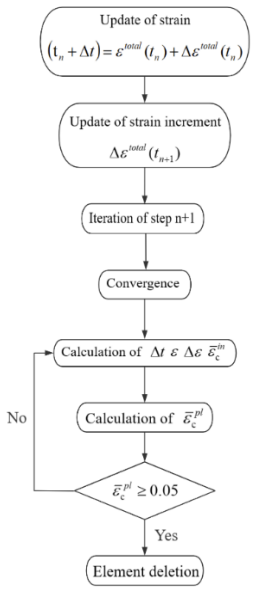

Figure 6. Flow chart of SC damage destruction

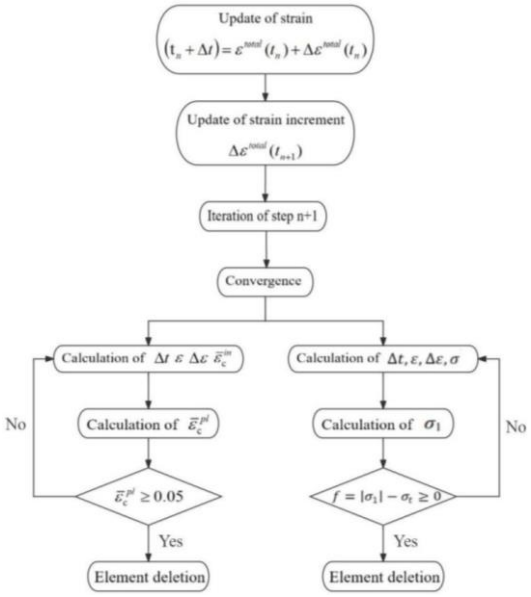

Figure 7. CFRP-SC damage destruction flow chart

3. Analysis of numerical simulation results

Concrete columns will be cracked, deformed and damaged during the stress process, resulting in the decline of material strength, stiffness and other properties, and the damage accumulated to a certain extent will cause structural damage. The working process of concrete structure is the crack damage accumulation process [16]. Therefore, it is of great importance to accurately grasp the damage accumulation process of the structure for the evaluation of member performance. In this paper, the damage evolution process of CFRP-SC will be discussed from the perspectives of damage pattern, vertical displacement, and stress.

3.1. SC destruction analysis

The concrete study object of prismatic cylinders with strength class C35. The damage factor of the model is very small when the vertical displacement U < 0.76 mm. The damage factors of the column units show slight differences. In the range of U > 0.76 mm, the damage factors of the column ends, and the column units gradually increased with the increase of load. As the model applied stresses approached the peak stress, member damage appeared on the surface and inside the concrete model, first at the end of the column. Subsequently, microcracks appeared on the columns. In the later stages of loading, the early microcracks gradually expanded and connected. Finally, the concrete model was sheared. The shear cracks were at approximately 45° to the concrete cross section. The shear crack runs through the entire model (Fig. 8).

SC damage begins with crack extension and ends with the damage of the SC as a whole. At the early stage of loading (U<0.76mm), the stresses at the two ends of the fissure increased continuously, and the phenomenon of stress concentration appeared. At this time, the maximum Mises stress is 27.11 MPa, and the maximum principal stress is 1.88 MPa. With the increasing vertical load, the unit cell at the tip of the fissure is the first to reach the damage condition. The crack extension is mainly along the oblique 45° direction, all perpendicular to the crack. At the late stage of loading (U>2.64mm), the number of units around the fissure that reach the damage condition increases, and the fissure continues to expand, eventually forming a macroscopic crack.

Some areas on the upper and lower sides of the crack are in tension (Fig. 8), and the maximum tensile stress concentration area is near the end of the crack. With the increase of vertical stress, the crack expanded and the distribution of tensile stress inside the specimen changed. At the same time,

with the increase of load, the maximum principal stress value is increasing, and the concentration is more obvious.

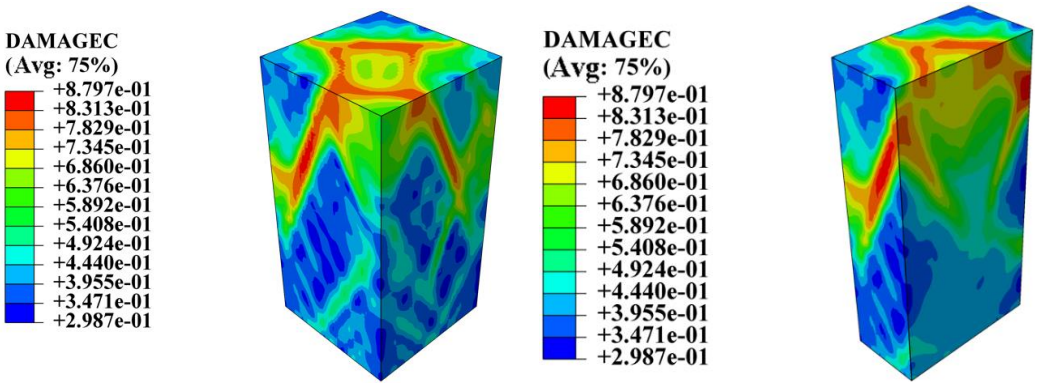

(a) Uncut (b) Y-axis cross-section

U=0.76mm

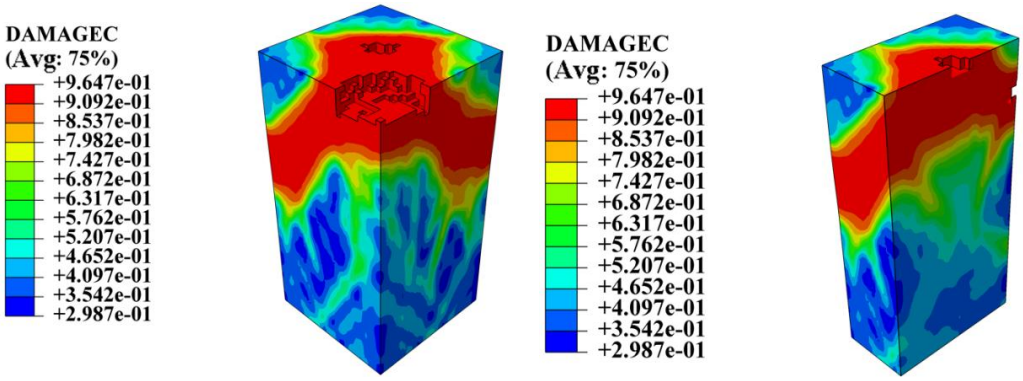

(a) Uncut (b) Y-axis cross-section

U=2.64mm

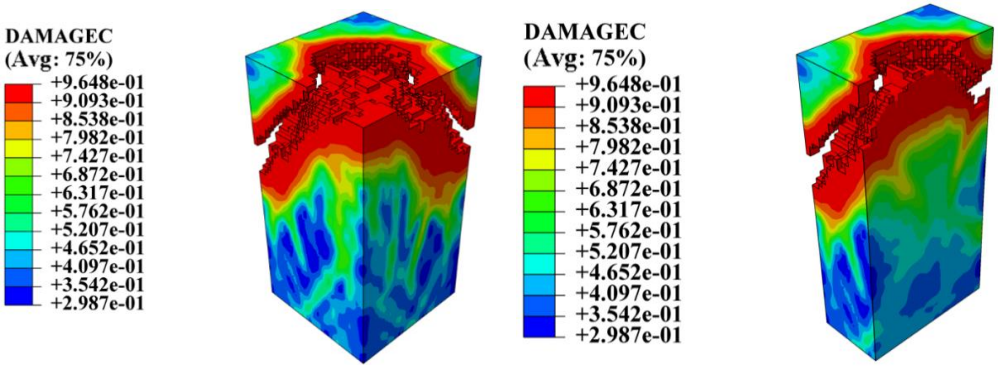

(a) Uncut (b) Y-axis cross-section

U=4.64mm

Figure 8. SC damage map

3.2. CFRP-SC destruction analysis

Under vertical loading, the cell is recognized as damaged and deleted, i.e., it is dropped from the iterative calculation for the next loading step. This iterative calculation is repeated until the calculation terminates when the residuals of the calculated internal forces in all cells satisfy the maximum tensile stress criterion, and the stress and strain results of the cells are output. In this section, the maximum tensile stress criterion is embedded in the VUSDFLD subroutine to simulate CFRP-SC in uniaxial compression test.

When U = 0.60 mm, the tensile stress of CFRP fibers reaches the tensile strength value and is subsequently destroyed. However, residual confining stresses existed on the surface of the concrete

restrained by the ties. With the increase of displacement, the member reaches the critical value of damage being destroyed in a large area. The cloud plots show that the damage of the units located at the CFRP fibers is low, while the damage is high in other parts of the model. This is due to the fact that the residual confining stresses on the model surface still inhibit crack extension after the CFRP fiber ties lose their restraining ability. Finally, shear damage occurred in the restrained concrete. The shear crack was approximately 45° from the concrete cross-section (Fig. 9).

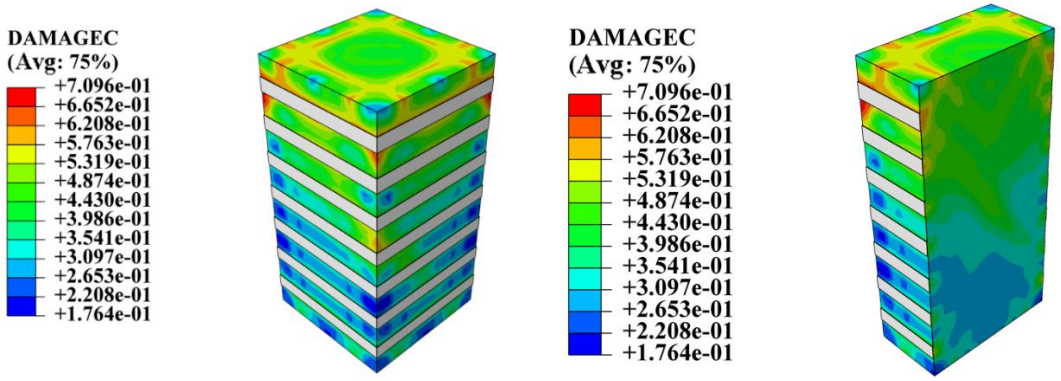

(a) Uncut (b) Y-axis cross-section

U=0.60mm

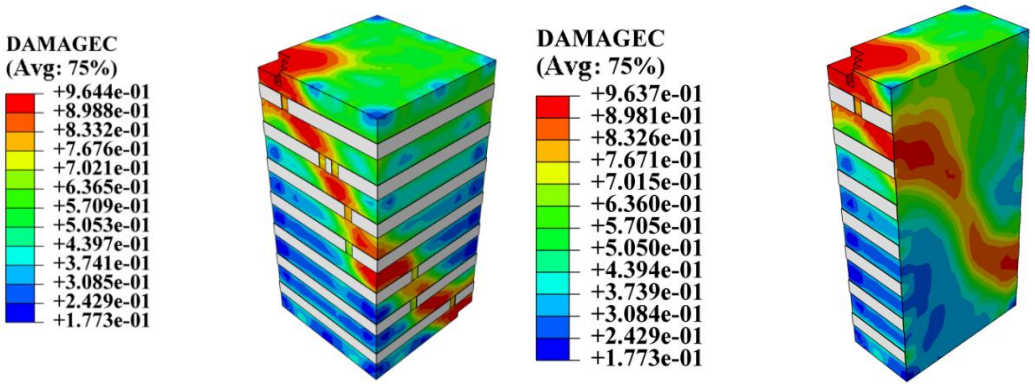

(a) Uncut (b) Y-axis cross-section

U=1.28mm

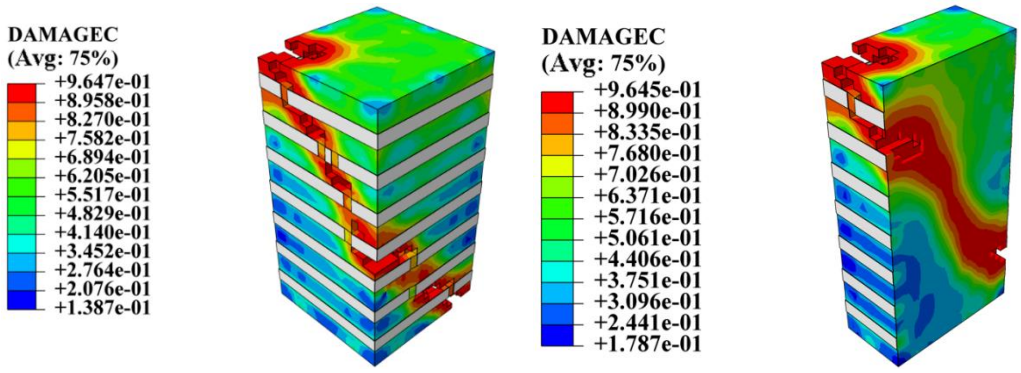

(a) Uncut (b) Y-axis cross-section

U=2.58mm

Figure 9. CFRP-SC damage map

At the early stage of loading, the constraining force provided by the CFRP fibers effectively prevented the increase of the concrete unit damage factor, and the unit damage factor increased slowly; in the middle stage of loading, the constraining CFRP fibers reached the tensile strength, and lost the role of constraining damage. Residual stresses existed on the concrete surface, which inhibited the crack expansion; in the late loading stage, the column unit damage formed a shear crack. The crack was at an angle of 45° with the column section, and the crack width was narrow. With the increase of

loading, the maximum principal stress value is increasing and the concentration is more obvious, up to 2.70MPa.

3.3. Stress-strain curves

Through the stress-strain diagram (Fig. 10), the peak SC compressive strength is 32.46 MPa, at which time the strain is 2.34×10^{-3}; the peak CFRP-SC compressive strength occurs when the strain is 2.55×10^{-3}, and the peak value reaches 36.48 MPa. SC members in the process of compression, with the increase in stress cracks from the emergence of the continuous development of the internal energy continues to accumulate, and when the stress value is greater than the SC compressive strength, the SC undergoes damage. After that point, the cracks continue to develop and expand, eventually forming macroscopic cracks. The slope of the stress-strain curve and the modulus of elasticity of SC in the restrained state of CFRP fibers are larger than those of unconstrained SC, which indicates that CFRP improves the strength of the member as well as the ductility of the member.

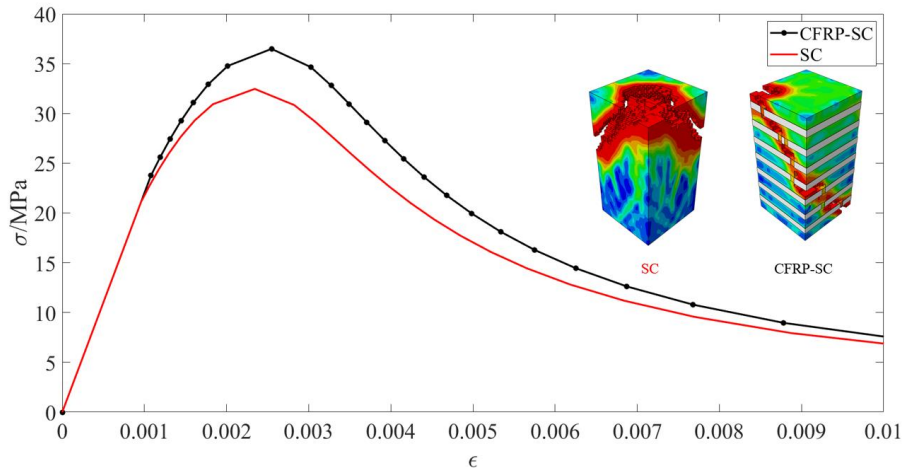

Figure 10. Stress-strain curve

4. Conclusion and outlook

In this paper, the axial compressive performance of CFRP-SC is simulated. The main conclusions are as follows:

(1) The reinforcement of CFRP-SC has a significant effect on the resistance to shear. Compared with the SC not restrained by CFRP fibers, the restrained members obviously have slow damage development. CFRP fibers can effectively improve the shear strength and stiffness of the columns, thus increasing the stability of the columns under shear loading.

(2) CFRP has an obvious improvement on the uniaxial compression performance of SC, showing good durability, which can improve the load carrying capacity of the column, and the wrapped CFRP-SC cracks are narrower under the same displacement loading, showing better ductility and toughness. Through the constraint of CFRP fibers, the members can still maintain high strength and stability under long-term loading.

References

[1] Liu Zhe, Mu Yulong, Hu Qing, et al. Research on application technology of SC engineering optimization [J]. Concrete World, 2023 (09): 64-67.

[2] ZHAO Yi; WU Xiao; Fu Qiang. Finite element simulation of flexural resistance of CFRP reinforced concrete beams [J]. Concrete, 2023, (10): 37-41.

[3] CHEN Ruilin, LI Kang, DONG Qi, et al. Numerical simulation of dynamic response analysis under blast impact of CFRP reinforced concrete slab [J]. Journal of Railway Science and Engineering, 2020, 6 (17): 1517-1527.).

[4] HUANG Liang; LI Yifan; LUO Cheng. Study on axial compressive properties of BFRP-reinforced sea sand recycled concrete columns [J]. Concrete, 2023, (10): 12-16+20.

[5] ZHAO Yi; WU Xiao; Fu Qiang. Finite element simulation of flexural resistance of CFRP reinforced concrete beams [J]. Concrete, 2023, (10): 37-41.

[6] Bai Song; XU Jinsheng; Xin Ming; LU Ziqi; WANG Yong. Analysis of basic mechanical properties of SC in fiber-reinforced seawater [J]. Journal of Lanzhou Institute of Technology, 2023, 30 (05): 16-19.

[7] Zhu Deju; Zhong Weilin; XU Zhenqin; LIU Zhijian; GUO Shuaicheng; LI Anling. Impact Resistance of Seawater SC Beams Enhanced by BFRP Bars [J]. Journal of Vibration and Shock, 2023, 42 (14): 220-228.

[8] Chen, J., Teng, J.G., and Ye, L.P. (2008). "Axial compressive behavior of concrete-filled FRP tubes and their CFRP-strengthened counterparts." Composite Structures, 84 (4), 310-324.

[9] Wu, Z., Zhang, Y., and Li, Z. (2018). "Experimental study on the compressive behavior of concrete-filled glass fiber-reinforced polymer tubes with CFRP confinement." Construction and Building Materials, 158, 506-517.

[10] Shi, Q., and Zhang, J. (2020). "Experimental study on the behavior of CFRP-confined concrete-filled square steel tubular columns." Construction and Building Materials, 259, 119411.

[11] ZHOU Fen, CHEN Yaman, ZHU Deju. Study on shear performance of ultra-high performance seawater SC beam with FRP bar [J/OL]. Journal of Hunan University (Natural Science Edition): 1-10 [2023-08-23].

[12] Wang, H.; Shang, S.; Zhou, H.; Jiang, C.; Huai, H.; Xu, Z. Experimental and Numerical Study on Uniaxial Compression Failure of Concrete Confined by Nylon Ties. Materials 2022, 15, 2975.

[13] Xiao, H.; Zhang, K.; Du, J. Numerical Simulation Analysis of Uniaxial Compression Damage of Reinforced Concrete Columns Based on ABAQUS. Highlights Sci. Eng. Technol. 2023, 51, 113–118.

[14] Secondary development and research on fracture propagation of tunnel surrounding rock based on ABAQUS [J] Shaanxi Water Conservancy, 2023 (09): 14-16.

[15] GB50010-2010, Code for Design of Concrete Structures [S].

[16] Qi Mingtao; Shao Yongjian; HONG Yu. Study on eccentric compressive properties and damage analysis of high-strength reinforced shale ceramsite concrete columns [J] Concrete and cement products, 2023, (10): 61-65+71.